PNAS RESEARCH ARTICLE | CHEMISTRY

Quantifying the ultrafast and steady-state molecular reduction potential of a plasmonic photocatalyst

Christopher L. Warkentin[a] and Renee R. Frontiera[a,1]

Edited by Catherine Murphy, University of Illinois at Urbana-Champaign, Urbana, IL; received April 12, 2023; accepted September 15, 2023

Plasmonic materials are promising photocatalysts as they are well suited to convert light into hot carriers and heat. Hot electron transfer is suggested as the driving force in many plasmon-driven reactions. However, to date, there are no direct molecular measures of the rate and yield of plasmon-to-molecule electron transfer or energy of these electrons on the timescale of plasmon decay. Here, we use ultrafast and spectroelectrochemical surface-enhanced Raman spectroscopy to quantify electron transfer from a plasmonic substrate to adsorbed methyl viologen molecules. We observe a reduction yield of 2.4 to 3.5% on the picosecond timescale, with plasmon-induced potentials ranging from −3.1 to −4.5 mV. Excitingly, some of these reduced species are stabilized and persist for tens of minutes. This work provides concrete metrics toward optimizing material–molecule interactions for efficient plasmon-driven photocatalysis.

plasmonics | photocatalysis | Raman spectroscopy

Significance

Plasmonic materials have been touted as ideal photocatalysts due to their extremely large optical cross-sections and ability to generate uniquely energetic nanoscale environments. However, many reports of plasmon-driven chemistry are phenomenological, and we lack the mechanistic understanding and quantitative metrics to rationally advance the efficiency, selectivity, reaction scope, and turnover number of these catalysts. Numerous articles in the past decade cite photoinduced electron transfer as the primary mechanism for plasmon-driven photocatalysis. However, the community was lacking basic metrics such as "how many molecules get transiently reduced?" and "how much energy do plasmon-derived hot electrons contain?" Here, we provide these values for a plasmonic substrate and validate a methodology that can be applied to a range of coupled plasmonic-molecule systems.

Using light, we can generate charges in materials (1) that can be collected for a range of useful applications, including pivotal technologies for sustainable energy generation and green catalysis. Alongside other exciting prospects, like quantum dots and 2D MXenes, (2, 3) plasmonic surfaces have shown promise for their ability to harness energy from light and drive a range of chemical reactions in nearby molecules (4, 5). Plasmonic materials support a coherent oscillation of electrons known as a localized surface plasmon resonance (LSPR). LSPRs can have energies in the visible and near-infrared regions of the electromagnetic spectrum, with their excitation leading to nanoscale confinement of light and generation of energetic, or hot, nonequilibrium charge carriers (6, 7). One can easily tune the frequency-dependent response of a plasmonic material by modifying its structure, dielectric properties, and surroundings (8). However, less is understood about how this tunability can be used to predictably modify specific plasmon-driven chemical reactions. This is made particularly difficult by the fact that we lack a molecular perspective on how these reactions proceed.

In recent decades, much progress has been made toward understanding fundamental properties of plasmon-generated charge carriers. Certainly, the field has gained a clearer understanding of their lifetimes (9, 10), explored methods to inhibit hot carrier relaxation (11–13), and grown a library of chemical reactions that are likely driven by plasmon-generated electrons or holes (14). Despite these advances, direct observation of plasmon-to-molecule charge transfer remains elusive, let alone measurement of the time-dependent plasmon reduction potential or yields and rates of these reactions. Monitoring the molecular dynamics involved in these processes and quantifying the energy of plasmon-generated carriers would provide the metrics by which excitation parameters, material characteristics, and molecular orientation can be mechanistically linked to the efficiency and yield of hot carrier transfer. This mechanistic understanding would provide insight into the rational design of plasmon-molecule photoredox pairs in the future.

Time is a critical factor when trying to understand plasmon-driven reactions. Both plasmon decay and molecular change occur over periods of femtoseconds to picoseconds. However, our current understanding of how molecules react to the highly energetic plasmonic environment on this ultrafast timescale is lacking. In addition, plasmon-molecule dynamics in the ultrafast and steady state can vary significantly. While charge carrier lifetimes typically occur on the picosecond timescale (9, 10), structural transformation of a plasmonic substrate, changes in molecular orientation, and irreversible chemical change can have more persistent, long-lived, effects on the ensemble profiles of molecular vibrations. Therefore, it is necessary to explore both of these temporal regimes—the ultrafast and steady state—in order to have a full picture of the dynamics at play.

Author contributions: C.L.W. and R.R.F. designed research; C.L.W. performed research; C.L.W. and R.R.F. contributed new reagents/analytic tools; C.L.W. and R.R.F. analyzed data; and C.L.W. and R.R.F. wrote the paper.

The authors declare no competing interest.

This article is a PNAS Direct Submission.

[1]To whom correspondence may be addressed; Email: rrf@umn.edu.

This article contains supporting information online at https://www.pnas.org/lookup/suppl/doi:10.1073/pnas.2305932120/-/DCSupplemental.

Published October 24, 2023.

In order to examine plasmon-mediated chemistry from a molecular perspective, we use ultrafast and steady-state surface-enhanced Raman spectroscopy (SERS) as our primary tool (15–18). SERS is a valuable spectroscopic technique that takes advantage of regions of enhanced electromagnetic fields on plasmonic substrates to amplify otherwise weak Raman scattered signal from molecular vibrations, typically on the order of 10^5 to 10^8 times (19). Time-dependent SER spectra can be used to gather dynamic information about plasmon-molecule systems. Continuous wave pump-probe SERS has been used on numerous occasions by van Duyne and others as a tool to monitor plasmon-driven charge transfer (20–22). This technique has been used to understand a number of plasmon-molecule systems in the steady-state using continuous wave lasers but does not provide information related to the pump/probe temporal offset or molecular change that occurs on the fs–ps timescale of plasmon decay. With ultrafast SERS, we pump the LSPR of the plasmonic material with a ultrashort laser pulse and use a second pulse to probe the molecular SERS response at various time delays relative to the pump. We have previously used this technique to better understand plasmonic heating (16), charge delocalization (15, 17), and energy transfer on the ultrafast timescale (18).

In this work, we use ultrafast SERS to track plasmon-mediated electron transfer from a molecular perspective. We pair a gold film over nanosphere (AuFON) plasmonic substrate (23–25) with the well-known redox indicator, methyl viologen (MV). MV has been the subject of interest for a variety of electrochemical studies that take advantage of the SERS effect, owing to its easily reversible transitions between the dication, radical cation, and fully reduced states (26–29).

Plasmon-driven reactions are often governed by light-driven surface potentials, which can be evaluated using electrochemistry (30). The combination of electrochemical techniques and SERS has been used widely for the identification of electrochemically generated surface species and found unique applications toward quantifying electrochemical heterogeneity, site specificity, and plasmon-generated potentials for nanostructures in the steady state (31, 32). Here, we apply spectroscopic methods to characterize how the vibrational modes of MV change—in both the ultrafast and steady state—when photochemically reduced on an AuFON surface. When we excite the plasmon resonance in the AuFON-MV system, electrons required to drive the reduction process are generated rapidly and we observe nonequilibrium changes to these MV vibrational markers using ultrafast SERS. Clear changes in these vibrational motions reveal a transient increase in reduced MV species on the fs–ps timescale. This transformation occurs simultaneously with the plasmon excitation and can be attributed to transfer of plasmon-generated electrons between the plasmonic substrate and adsorbed MV. Furthermore, correlation of spectroelectrochemical and ultrafast measurements allows us to quantify both the reducing power of the AuFON substrate and relative changes to the population of MV redox moieties.

In order to take advantage of the inherent tunability of plasmon-molecule systems, detailed reaction metrics must be correlated with physical properties of the system—excitation power, plasmonic resonance/excitation frequency, nanostructure, and metal–molecule hybridization (e.g., adsorption geometry). Greater predictability for how reaction mechanisms change through the modification of these physical parameters would allow for dynamic control of plasmon-driven chemistries. Here, we describe a method that provides the readout necessary for calibrating these physical variables through the systematic quantification of plasmon-generated potentials as well as the rates and yields of the reactions they drive.

Results and Discussion

We tuned the LSPR of our AuFON substrates by modifying the silica sphere size and Au thickness to match the ∼1,040-nm excitation wavelength of the ultrafast SERS setup and characterized their optical response using vis-NIR extinction spectroscopy (*SI Appendix*, S1). We configured our ultrafast and spectroelectrochemical SERS setup to collect photons in a range of Raman frequencies between 486 cm^{-1} and 2,220 cm^{-1}, allowing us to probe a broad span of MV molecular vibrations.

Spectroelectrochemical SERS of MV. In order to clearly assign vibrational changes to MV following an interaction with plasmon-generated charge carriers, we first performed spectroelectrochemical SERS (SEC-SERS) measurements on our experimental plasmon-molecule system. Surface-enhanced vibrational signatures of molecules on plasmonic materials can vary significantly from those in the gas or solution phase, particularly due to molecular binding configuration or orientation relative to the plasmonic near field (33). Furthermore, ground state SER spectra of MV on AuFON substrates contain a mixture of MV redox species due to spontaneous charge transfer processes (28). Thus, careful quantification of redox potentials and vibrational frequency shifts on the same substrates used for ultrafast SERS is crucial for measuring photoinduced plasmonic reduction potentials.

To closely correlate our SEC and ultrafast SERS measurements, we performed all SEC-SERS measurements using a homemade AuFON working electrode and the same ∼1,040-nm picosecond laser beam used for ultrafast SERS (Fig. 1*C*). We placed the AuFON electrode in a 1-mm-thin layer quartz cell (Pine Research, RRPG094) containing 0.1 mM $MVCl_2$ solution in 0.1 M KCl—with Ag/AgCl reference and gold wire counter electrodes. Full details of the SEC methods and setup and are available in *SI Appendix*. We determined the reduction potentials for MV on the AuFON surface using cyclic voltammetry (CV), with an ${E_{r1}}^0$ ($MV^{2+} \rightarrow MV^{\bullet+}$) of ~ -0.66 V and ${E_{r2}}^0$ ($MV^{\bullet+} \rightarrow MV^0$) of ~ -1.06 V (Fig. 1*B*), in good agreement with previously reported reduction potentials (Fig. 1*B*) (28).

We then stepped through ${E_{r1}}^0$ and ${E_{r2}}^0$ in increments of 25 mV, allowing the system to equilibrate for 60 s before taking SER spectra of MV at the electrode surface (Fig. 1*A*). Starting at the onset of the $MV^{2+} \rightarrow MV^{\bullet+}$ transition (~ -0.59 V), an overall increase in SER signal is observed. This increase in signal is likely due to preresonant Raman signal enhancement. A transition in the MV inter-ring angle from ∼43° to planar may also result in a significant increase in the overall Raman cross-section for most MV vibrational modes (34). As we move through the $MV^{\bullet+} \rightarrow MV^0$ (~ -0.9 V) transition, there is a clear increase in the intensity of the MV^0 CNC stretch/in-plane ring deformation at 990 cm^{-1} (Fig. 1*A*, green trace), the inter-ring stretch at 1,535 cm^{-1}, and the CNC/CCC ring stretch at 1,660 cm^{-1} (*SI Appendix*, S11) (34, 35). Notably, the 1,020-cm^{-1} vibrational mode (Fig. 1*A*, blue trace), corresponding to the $MV^{\bullet+}$ CNC stretch/in-plane ring deformation, decreases in intensity over this potential range. From this analysis, we determine that the reduction of $MV^{\bullet+}$ to MV^0 results in an increase in the ratio of the 990-cm^{-1} (MV^0) and 1,020-cm^{-1} ($MV^{\bullet+}$)

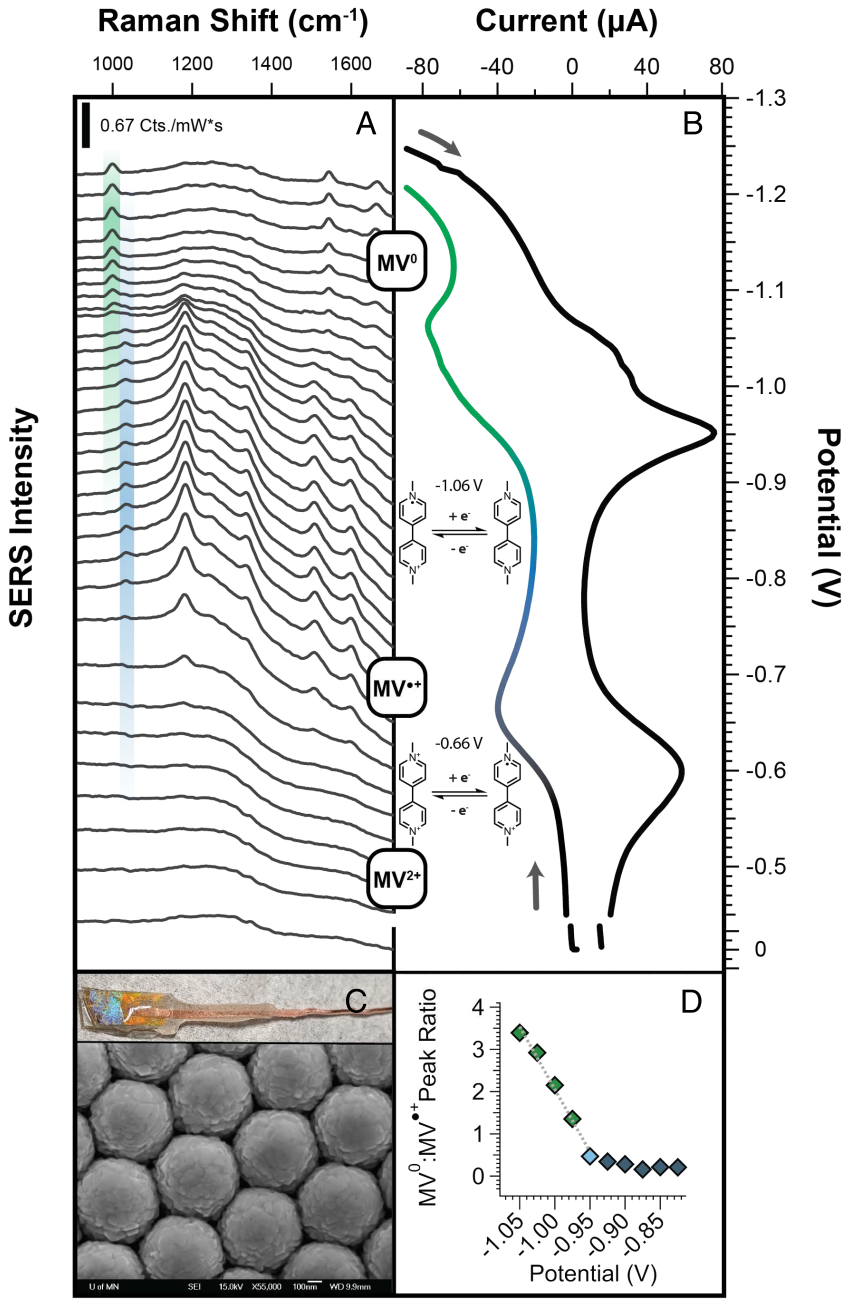

Fig. 1. (*A*) SER spectra of methyl viologen as a function of applied potential. As the first and second reduction potentials are crossed, ring deformation modes at 1,020 cm^{-1} ($MV^{\bullet+}$) and 990 cm^{-1} (MV^{0}) increase, respectively. (*B*) CV of $MVCl_2$ solution at AuFON working electrode. We determined the first and second redox potentials to be ~ −0.66 V and −1.06 V, respectively. (*C*) Homemade AuFON working electrode and SEM image of AuFON structure. (*D*) Calibration plot of 990 cm^{-1} : 1,020 cm^{-1} peak ratios as a function of applied potential.

ring deformation modes, which can be used as a clear marker for charge transfer events that might be observed in our ultrafast experiments. Importantly, beyond the qualitative identification of a charge transfer event, the combination of electrochemical and vibrational information allows us to correlate changes in the $MV^{\bullet+}$: MV^{0} ring deformation peak ratio with relative changes to populations of MV redox states and potentials generated from LSPR excitation (*SI Appendix*, S2–S4 and Fig. 1*D*).

Ultrafast SERS of MV on AuFON. For ultrafast measurements, we applied 40 μL of 1 mM methyl viologen dichloride (Sigma Aldrich, 98%, 75365-73-0) in ethanol (Decon, 95%) to each of the AuFON substrates and allowed the solvent to evaporate under ambient conditions. It should be noted that differences in sample preparation methods between SEC and ultrafast SERS result in ~ 40 cm^{-1} shift in their observed ring deformation vibrational frequencies, likely due to variation in the dielectric function of their surrounding media, and/or MV adsorption geometry. Both the method by which molecules are added to the surface and the solvent environments are different for samples used in ultrafast and EC-SERS experiments. Therefore, this shift may be due to changes in the local nanoscale dielectric environment, differences in molecular packing, or the impact of the femtosecond pump pulse that is only present in the ultrafast experiments. The presence of the pump pulse may impact restructuring of the surface, provide a local electric field, or

drive changes in the molecular adsorption geometry. However, it is most important to note that most of the signal in both cases comes from the highest enhancing regions of these highly heterogeneous substrates (36). In order to avoid artifacts of laser-driven restructuring in the ultrafast measurements, we applied $MVCl_2$ to the AuFON, and allowed the system to equilibrate under laser excitation before running experiments, exposing the substrate to both the pump and probe for 5 min (37). After the equilibration step, we excited the LSPR of the AuFON-MV system with a 1,037-nm, 200-fs pump pulse, and collected the spontaneous MV SERS signal via 1,041-nm, 2-ps probe pulse at time delays ranging from −50 to 50 ps (Fig. 2A).

In Fig. 2*B*, we present ultrafast SERS data showing the molecular response of MV before and after plasmon excitation. At the *Bottom* of the figure, we display a typical ultrafast SER spectrum where the pump and probe pulses are offset by −50 ps. We refer to this as our ground, or unperturbed, state of the AuFON-MV system (more details in *SI Appendix*). A comparison of $MV^{\bullet+}$ and MV^0 ring deformation mode intensities between SEC-SERS data (Fig. 1*A*) and the ground state MV spectrum (Fig. 2*B*) clearly show that the MV redox species in these most enhanced regions is a mixture of $MV^{\bullet+}$ and MV^0 (Fig. 2*B*). Although there is some variability between experiments, we estimate an initial MV^0 : $MV^{\bullet+}$ ratio of ∼1:1. This initial population of MV redox states is likely due to a combination of spontaneous charge transfer to MV^{2+} as it is adsorbed to the AuFON surface, subsequent LSPR excitation during the equilibration step, and/or impacts from the probe pulse (28).

Examining the time-dependent spectra in our ultrafast SERS experiments, we clearly observe transient changes in MV redox state populations. In Fig. 2*B*, we display our ultrafast SER spectra as a change in intensity with respect to the unperturbed sample,

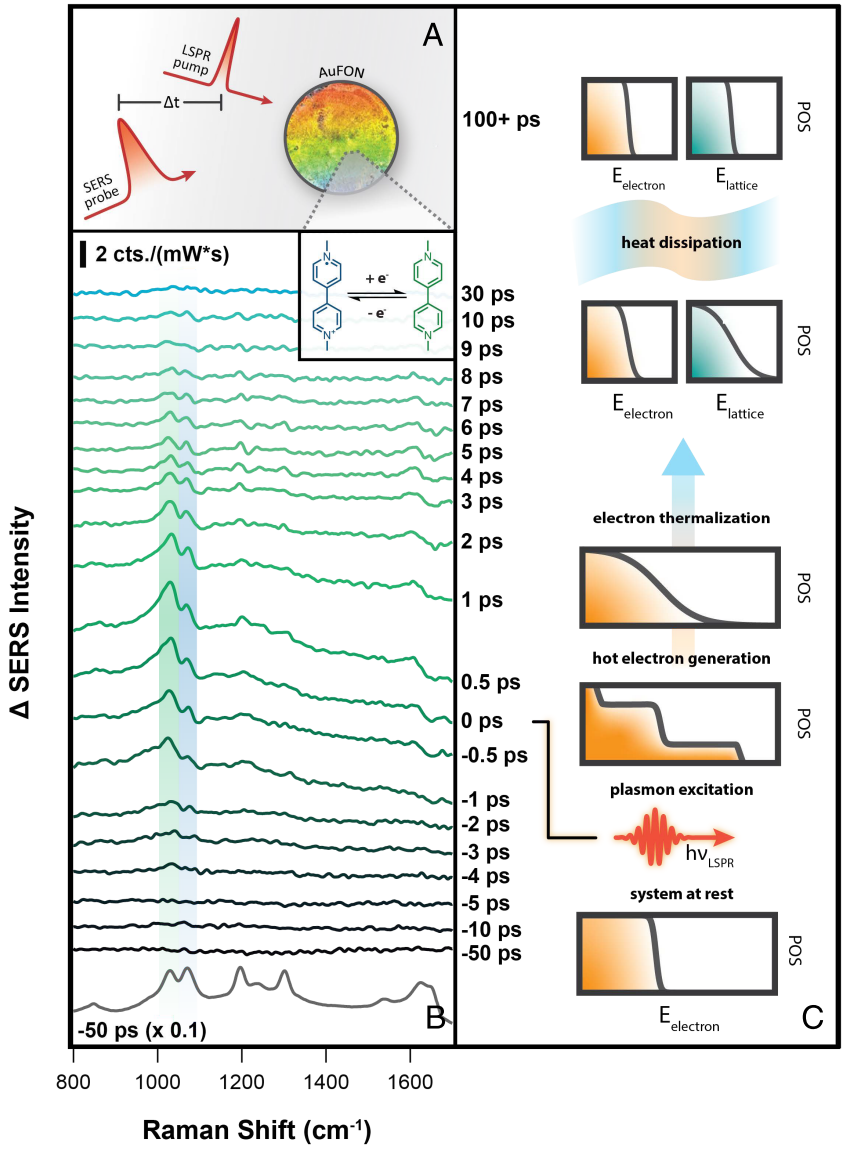

Fig. 2. (*A*) Schematic of the ultrafast SERS experiment. We excite the LSPR using a pump pulse and observe molecular change at various time delays with a spontaneous SERS probe. (*B*) Representative ground state addition ultrafast SERS experimental spectra of $MVCl_2$ on AuFON (10.6 W/cm^2 pump, 13.6 W/cm^2 probe). A mixed $MV^0/MV^{\bullet+}$ ground state population evolves after the LSPR excitation, where we observe an increase in the relative MV^0 (green) : $MV^{\bullet+}$ (blue) ratio. This change is proof of a plasmon-driven charge transfer from AuFON to $MV^{\bullet+}$. (*C*) Overview of energy dissipation following LSPR excitation. After excitation, free electrons take on a nonequilibrium distribution of energies (10 to 100 fs). These electrons thermalize through electron–electron/electron–phonon scattering and interactions with nearby molecules (1 to 10 ps). Phonon excitation increases the lattice temperature, which eventually equilibrates with the bath (100+ ps).

allowing us to more clearly visualize small changes throughout the spectral evolution. Here, negative timepoints represent when the SERS probe interacts with the sample before the LSPR pump, and positive timepoints represent when the probe interacts with the sample after the pump. As the pump excites the LSPR, we see that the intensity of the MV^0 ring deformation mode (1,030 cm^{-1}, green) clearly increases with respect to the $MV^{\bullet+}$ ring deformation mode (1,071 cm^{-1}, blue). The positive change in the MV^0 : $MV^{\bullet+}$ peak ratio is distinct evidence of a plasmon-initiated electron transfer from the AuFON to nearby $MV^{\bullet+}$ on the ultrafast timescale. We note that a small increase in the MV^0 : $MV^{\bullet+}$ peak ratio is observed before time zero, which we attribute to spatial chirp of our pump beam, resulting in an asymmetric cross-correlation of our pump and probe (*SI Appendix*). Based on ultrafast theoretical and experimental results of plasmonic gold lattice and electron temperatures (38–40), a large portion of the initially photoexcited electron temperatures should easily exceed the reduction potential.

We performed ultrafast SERS measurements over a range of LSPR pump flux from 4.87 to 10.6 W/cm^2. At each pump flux, we performed 10 measurements in unique sample positions, spanning 4 individually prepared AuFON substrates. We calculated figures of merit for each dataset individually and average the results at each pump flux, with y-value error given as the propagation of uncertainty—predominately influenced by uncertainty in the ultrafast SERS and SEC SERS peak fits (Fig. 3*B* and *SI Appendix*, S8). Error in average flux is propagated from the SD of measured power across all 10 experiments and the measured pump area. We observe a maximum increase in the average MV^0 : $MV^{\bullet+}$ peak ratio of ~ 0.1 to 0.15 over the full range of applied pump flux. Using calibrations from the SEC-SERS MV^0 : $MV^{\bullet+}$ peak ratios (*SI Appendix*, S3), we estimate an average pump flux dependent change in MV^0 population of ~ 2.4 to 3.5% within the picosecond time resolution of our measurement (Fig. 3*B*). The observed transient reduction increases linearly with applied pump power, with a slope of ~ 0.19 % increase in MV^0 per W/cm^2. Notably, a shoulder feature (1,017 cm^{-1}, See *SI Appendix*) red-shifted from the 1,030-cm^{-1} MV^0 ring deformation peak also increases in intensity, indicating that the plasmon-generated electrons leave a portion of the reduced MV^0 molecules in excited vibrational states—equivalent to an electrochemical overpotential (Fig. 3*D*). Our kinetic analysis of this excited vibrational feature suggests that approximately 3% of reduced MV^0 molecules occupy vibrationally excited states at time zero (*SI Appendix*, S12).

In addition to quantifying the percent of molecules reduced, we can correlate the observed change in the MV^0 : $MV^{\bullet+}$ peak ratio with potentials applied in our SEC-SERS experiment. In this way, we can determine the plasmon-generated potential experienced by MV on the AuFON surface following plasmon excitation (*SI Appendix*, S4). Here, we observe an ensemble averaged plasmon-generated potential ranging from ~ −3.1 to

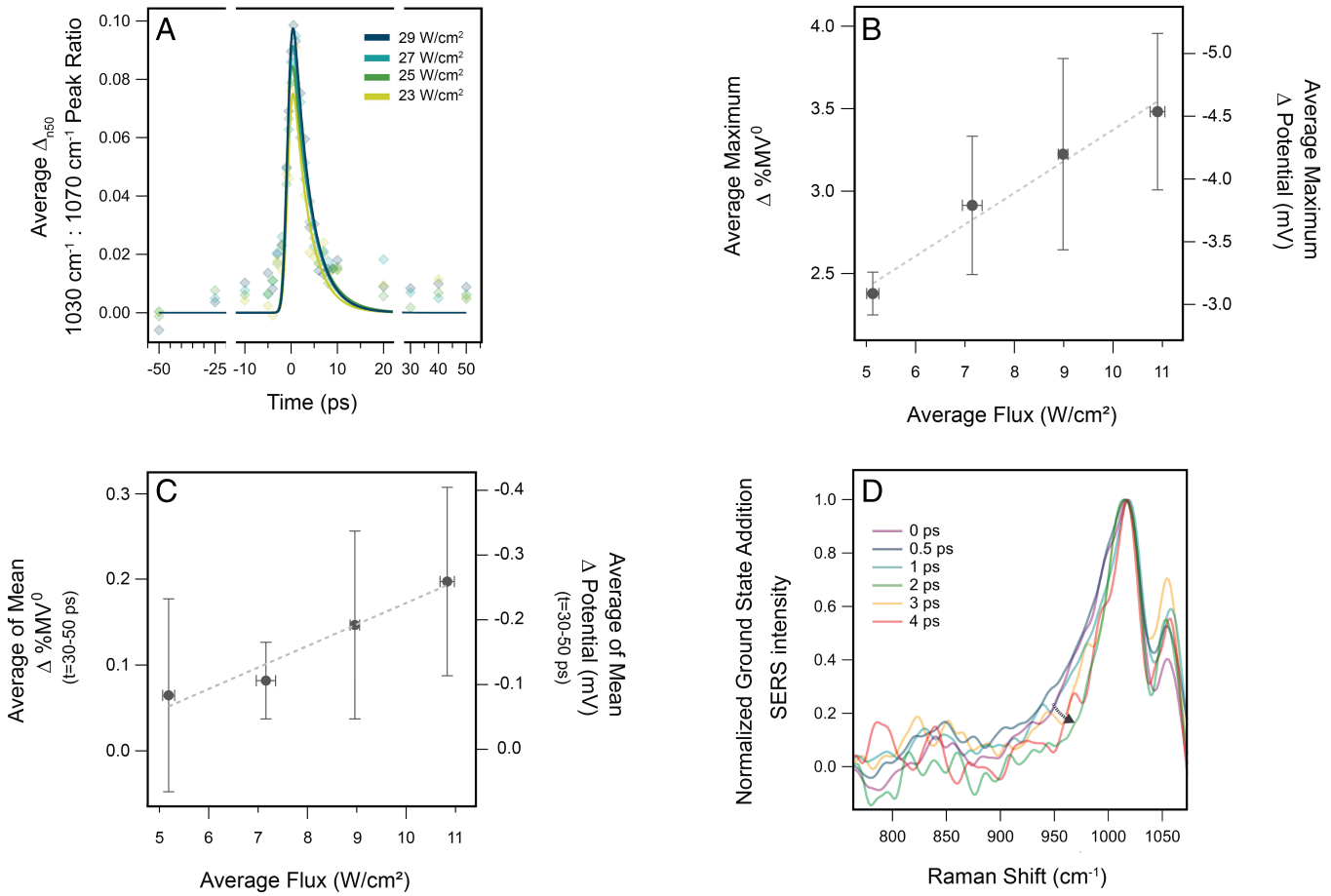

Fig. 3. (*A*) Average kinetic traces of 10 ultrafast SERS experiments at 4.87 to 10.6 W/cm^2 LSPR excitation flux. Correlation of ultrafast and SEC SERS measurements facilitates quantification of corresponding changes in $\%MV^0$ and electrochemical potential. These experiments lie in a linear regime for the dependence of the average maximum (*B*) and longer-lived (*C*) peak ratios on incident flux. (*D*) Transient signatures of excited vibrational states at 10.6-W/cm^2 pump power.

−4.5 mV, increasing linearly with LSPR pump power at a rate of ∼ 0.25 mV per W/cm^2.

A majority of the plasmon-generated MV^0 population quickly decays back to the ground state. This decay is comparable across all samples and applied flux, with an average lifetime over all experiments of 3.6 ± 0.3 ps. However, as seen in Fig. 3*A*, peak ratios at time points ranging from 30 to 50 ps are slightly elevated from the baseline, implying that there is a small population of reduced species that have much longer lifetimes.

Due to the small magnitude of the change in the MV^0 : $MV^{\bullet+}$ peak ratio, we could not extract lifetimes for these persistent reduced molecules with an acceptable degree of uncertainty. However, we were able to confirm the existence of this population through an analysis of the baseline offset at later time points (30 to 50 ps). We took the average of the mean of MV^0 : $MV^{\bullet+}$ peak ratios from 30 to 50 ps over all 10 experiments at each pump flux, with error calculated as described previously. We display the resulting analysis in Fig. 3*C*, where there is a significant increase from the initial peak ratio at these later time points (*SI Appendix*, Tables 3 and 4). The offset increases linearly with the incident flux of the LSPR pump, correlating with the power dependence for the maximum peak ratio. We see that ∼ 0.6 to 1.3 % of the MV^0 generated from plasmon excitation remains beyond the bulk lifetime of 3.6 ps. This fraction of reduced molecules remain in the enhanced regions of the AuFON for at least 50 ps but could remain longer.

Steady-State Plasmon-MV Dynamics. A great advantage of ultrafast SERS is that it not only allows us to observe ultrafast dynamics of plasmon-molecule systems but also gives us the ability to track chemical change in the system on the time scale of the entire experiment (∼ 25 min). We do this by reordering data for our ground state spectra in relation to acquisition order, rather than the pump/probe temporal offset. Interestingly, while we observe an increase in the MV^0 : $MV^{\bullet+}$ peak ratio on the ultrafast timescale (∼ 0.15, 10.6 W/cm^2 pump), over the longer timescale

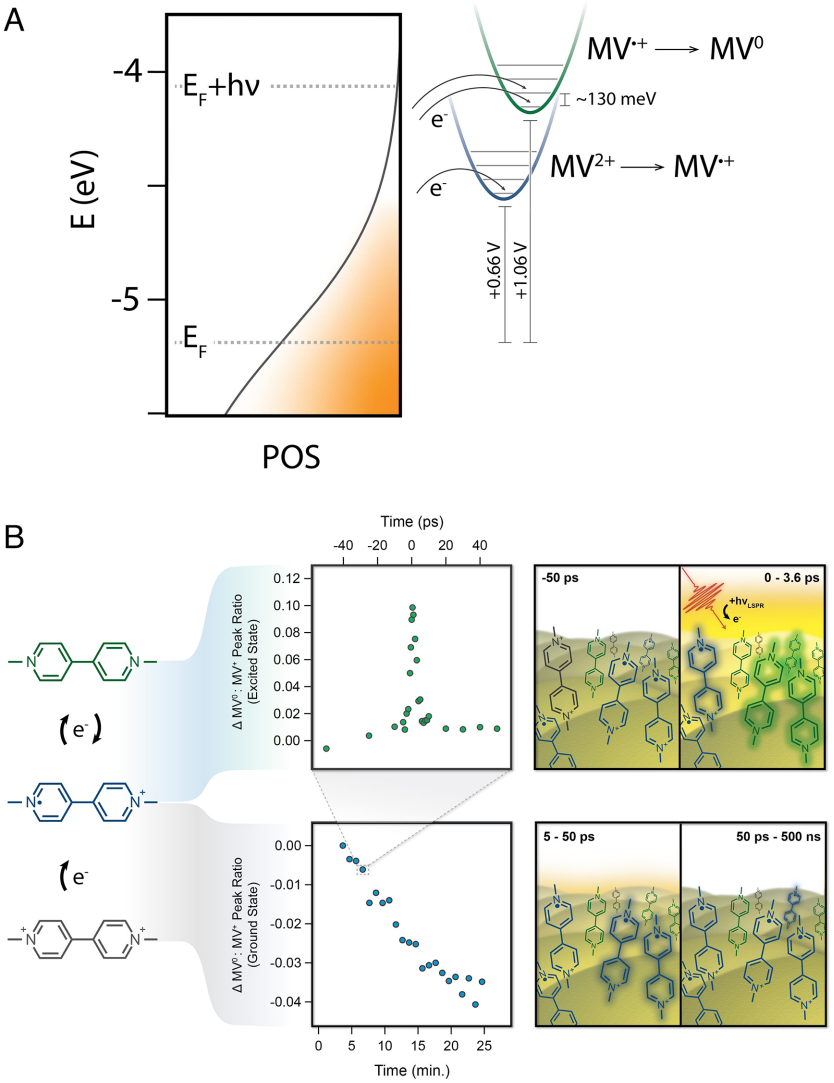

Fig. 4. (*A*) Depiction of plasmon-driven reduction of methyl viologen, as observed by ultrafast SERS. (*B*) Representation of interplay between ultrafast and steady-state time regimes. In the ultrafast measurements (*Top*), we observe a transient increase in [MV^0], and we infer a concurrent decrease in [MV^{2+}], with Δ [MV^0] >> Δ [MV^{2+}]. MV^{2+} does not have any observable spectral features in the 1,000 to 1,100 cm^{-1} region. The bulk of this MV^0 population decays over ∼ 3.6 ps, with ∼ 2% remaining for > 50 ps. However, conversion of MV^{2+} to $MV^{\bullet+}$ over the course of each ∼25-min experiment results in a net increase in [$MV^{\bullet+}$] over time (*Bottom*). These long-time dynamics are provided by the same ultrafast laser pulses used in the ultrafast experiments, in order to facilitate direct comparisons.

of the 25-min experiment, we measure an overall decrease in that ratio of ~ 0.04 (10.6 W/cm^2 pump). For comparison to the ultrafast kinetics, this translates to a change in the MV^0 : $MV^{\bullet+}$ peak ratio of $\sim 10^{-15}$/ps; on the order of one molecule per pulse. The decrease in peak ratio over the course of the experiment is smaller than the increase in the ultrafast regime, so any competition between these processes is negligible in our ultrafast kinetic analysis (Fig. 4). Nonetheless, we are able to quantify the aggregate effect that this has over tens of minutes, which implies a clear difference in reactivity between the ultrafast and steady-state time regimes for this plasmon-driven process.

We believe that this interesting dichotomy for reactivity between ultrafast and steady-state time scales may arise from the heterogeneity of binding geometries of methyl viologen on the AuFON surface. This surface is known to contain a range of areas with Raman enhancement factors spanning many orders of magnitude, attributed to the large heterogeneity of hot spot structures (36). This heterogeneity, as well as the tendency for the surface to restructure under weak light illumination, is common in gold plasmonic nanostructures (41) and represents a realistic surface for practical catalysts. Thus, there are a range of methyl viologen–binding geometries represented in our sample, of which a small subset may exist in a geometry or specific local environment that stabilizes the charge-transferred state. We propose that every time the LSPR is excited, a small portion of the radical cation population is transiently converted to the neutral species, which undergoes back electron transfer before the next pulse arrives (<500 ns). Simultaneously, a very small amount of the remaining dication is irreversibly reduced to $MV^{\bullet+}$. Because the change to the MV^{2+} population is so small, we overwhelmingly observe the transient reduction of $MV^{\bullet+}$ to MV^0 in the ultrafast regime. However, over the course of the 25-min experiment, we observe a net increase of the $MV^{\bullet+}$ population in the enhanced regions of the AuFON, owing to the aggregate conversion of MV^{2+} over billions of pulses (Fig. 4). While it is also possible that there is a thermally driven charge transfer mechanism responsible for this long-lived reduced state observed in the steady state, previous measurements from our group looking at molecular temperatures under very similar conditions show minimal heating in the ground state (16, 42). Therefore, we tentatively conclude that the existence of these very long-lived reduced species is not solely the result of a rise in steady-state temperature. This interplay between reactivity on the ultrafast and steady-state timescale provides a fresh perspective on tuning plasmon-driven chemistry—where, using pulsed excitation, one could envision perturbing ultrafast dynamics toward desired steady-state outcomes in ways that would not be possible with continuous wave excitation alone.

Importantly—in addition to this side-by-side analysis of ultrafast and steady-state plasmon-driven chemical change—we describe here a direct molecular measurement of plasmon-driven charge transfer on the timescale of hot carrier thermalization. We are able to perform correlative analysis of these data to quantify hot electron energies and relative changes to the redox state of MV. Beyond a simple observation of charge transfer, this quantification gives further insight into the nature of this plasmon-molecule system.

By pairing ultrafast SERS with SEC-SERS, we are able to quantify key values for the light-driven reduction of $MV^{\bullet+}$ to MV^0. Here, we observe a maximum reduction of $MV^{\bullet+}$ to MV^0 of ~2.4 to 3.5%. The fraction of molecules reduced in the enhanced region of the substrate likely have geometric orientations ideal for undergoing charge transfer (43). Some molecules may be reduced and then reoxidized on timescales faster than our instrumental response function and not included in the reduction potential calculation. We note that this extremely fast and short-lived reduction is likely not relevant for most plasmon-driven chemistries. Given the heterogeneity of binding sites on the AuFON surface, the relatively large reduction yield that we observe on this timescale is promising and suggests that there may be a range of binding configurations acceptable for undergoing charge transfer in this plasmon-molecule system.

The average lifetime for plasmon-reduced MV^0 is 3.6 ps—on the order of magnitude of past measurements for plasmon-generated electron thermalization (9, 10, 44). Interestingly, we observe that ~ 0.6 to 1.3 % the plasmon-generated MV^0 remain reduced for at least 50 ps. This small number of extremely long-lived reduced species is very relevant for chemical reactivity—especially considering reactions such as CO_2 reduction or ammonia synthesis, which require multiple reduction steps. This is certainly an exciting result, and a better understanding of how these reduced species are stabilized could aid in making use of this plasmon-molecule system to catalyze further reactions.

We suggest two origins for the stabilization of these reduced species. First, it is possible that a subset of the initially reduced species remain in a reduced state for tens of picoseconds. In this case, heterogeneity of the AuFON binding sites may provide sample geometries that maintain the charge transferred state. These persistent reduced species may be adequately spaced from adjacent MV molecules, making them less susceptible to electronic quenching through intermolecular relaxation (18, 45). Additionally, under ambient conditions, gold films are known to have a hydration layer on the scale of tens of nanometers, which may also play a role in stabilizing the reduced species through electrostatic interactions (46, 47). The second possibility is a thermally mediated process, where an increase in the temperature of the gold lattice facilitates charge transfer via a change in the gold Fermi level. Charge transfer is known to be moderately temperature dependent in methyl viologen (48). These thermally reduced species would likely be observed on the tens of picosecond timescale. Both of these mechanisms are consistent with the time-resolved growth observed in our ultrafast SERS measurements, but with the time resolution of this experiment we are not able to distinguish them. It is possible that higher time-resolution measurements with molecular specificity, such as surface-enhanced femtosecond stimulated Raman spectroscopy, (49) will be able to provide more insights into these mechanisms.

Using our molecular probe, we measure an ensemble averaged plasmon-generated potential, which varies from −3.1 to −4.5 mV depending on the flux of the LSPR pump. However, considering the potential difference of ~220 mV between MV^0 and $MV^{\bullet+}$ (Fig. 1*B*) and energy required to generate vibrationally excited MV^0 species (~126 meV), some electrons must have energies exceeding 340 meV (Fig. 3*D* and *SI Appendix*, S12). Notably, the ensemble average plasmon-generated potential measured in this study is approximately two orders of magnitude less than measured values in other recent work (32, 50, 51). For example, Yu and coworkers have recently reported a hot electron energy of 0.32 eV generated from continuous wave excitation of a gold nanosphere array. The potential observed in their work was observed through the plasmon-driven reduction of 4-nitrothiophenol, a small molecule with strong surface adsorption properties on Au (~50 to 100 kcal/mol) (52–54). Comparatively, MV is much larger and more loosely adsorbed

to the AuFON surface (~8 to 20 kcal/mol) (55–57). These differences likely play a role here, where molecular properties, adsorption, and relative electron affinity—in addition to possible variations in crystallinity of the metallic binding sites—can have a significant impact on the resistivity of the metal–molecule interface by changing the relative energy of the HOMO and LUMO of the molecule and the Fermi level and work function of the metal (58, 59). Importantly, the ultrafast/SEC SERS techniques show great promise toward correlating these factors with differences in observed plasmon-generated potentials on the ultrafast timescale.

Conclusion

In summary, we have shown that ultrafast SERS is well suited for monitoring plasmon-driven chemical processes and have provided direct evidence of plasmon-mediated charge transfer from a molecular perspective. Coupling ultrafast and spectroelectrochemical SERS has given us insight into the efficiency and magnitude of charge transfer in the AuFON-MV system, which is heterogeneous both in the structure of the AuFON and in the distribution of molecules on its surface. This work serves as a promising proof of concept, showing that our ultrafast SERS technique is sensitive enough to monitor and quantify molecular signatures of plasmon-driven charge transfer.

Moving forward, the correlation of ultrafast and spectroelectrochemical SERS analyses should allow for quantifiable relationships between plasmon-generated electrochemical potential and the physical characteristics of a plasmonic system, an invaluable tool for understanding and mitigating barriers to charge transfer across the metal–molecule interface. Next steps should focus on differentiating between the roles of molecule-surface adsorption and orientation as well as plasmon-generated carrier density in the efficiency of ultrafast and steady-state plasmon-driven charge transfer processes. In the future, we see ultrafast SERS as a promising tool to characterize and inform the modification of molecular ultrafast dynamics in plasmon-driven chemistries for desired steady-state outcomes.

Data, Materials, and Software Availability. All relevant raw data and analysis files have been submitted to Data Repository of the University of Minnesota. A persistent link is available at https://hdl.handle.net/11299/255747 (60).

ACKNOWLEDGMENTS. We thank Dr. James Brooks and Dr. Nathaniel Brandt for their work in building portions of the experimental setup and making some preliminary measurements of AuFON-MV systems. Portions of this paper were developed in Dr. Warkentin's thesis. Parts of this work were carried out in the Characterization Facility, University of Minnesota, which receives partial support from the NSF through the Materials Research Science and Engineering Center (MRSEC) (Award No. DMR-2011401) and the National Nanotechnology Coordinated Infrastructure ((NNCI) (Award No. ECCS-2025124) programs. Portions of this work were conducted in the Minnesota Nano Center, which is supported by the NSF through the NNCI under Award Number ECCS-2025124. We acknowledge the Minnesota Supercomputing Institute (MSI) at the University of Minnesota for providing resources that contributed to the research results reported within this paper http://www.msi.umn.edu. Air Force Office of Scientific Research under AFOSR Award No. FA9550-15-1-0022. Renewable Energy Commercialization Fellowship through the Institute on the Environment at the University of Minnesota.

Author affiliations: [a]Department of Chemistry, University of Minnesota, Minneapolis, MN 55455

1. A. B. Arons, M. B. Peppard, Einstein's Proposal of the Photon Concept-a Translation of the Annalen der Physik Paper of 1905. *Am. J. Phys.* **33**, 367–374 (1965).
2. F. P. García *et al.*, Semiconductor quantum dots: Technological progress and future challenges. *Science (New York, N.Y.)* **373**, 8541 (2021).
3. A. VahidMohammadi, J. Rosen, Y. Gogotsi, The world of two-dimensional carbides and nitrides (MXenes). *Science (New York, N.Y.)* **372**, 1581 (2021).
4. D. Devasia, A. Das, V. Mohan, P. K. Jain, Control of chemical reaction pathways by light-matter coupling. *Annu. Rev. Phys. Chem.* **72**, 423–443 (2020).
5. L. Zhou *et al.*, Quantifying hot carrier and thermal contributions in plasmonic photocatalysis. *Science* **362**, 69–72 (2018).
6. L. Novotny, B. Hecht, *Principles of Nano-Optics* (Cambridge University Press, Cambridge, United Kingdom, 2012).
7. A. Manjavacas, J. G. Liu, V. Kulkarni, P. Nordlander, Plasmon-induced hot carriers in metallic nanoparticles. *ACS Nano* **8**, 7630–7638 (2014).
8. K. L. Kelly, E. Coronado, L. L. Zhao, G. C. Schatz, The optical properties of metal nanoparticles: The influence of size, shape, and dielectric environment. *J. Phys. Chem. B* **107**, 668–677 (2003).
9. J. G. Liu, H. Zhang, S. Link, P. Nordlander, Relaxation of plasmon-induced hot carriers. *ACS Photon.* **5**, 2584–2595 (2018).
10. Y. Wang *et al.*, In situ investigation of ultrafast dynamics of hot electron-driven photocatalysis in plasmon-resonant grating structures. *J. Am. Chem. Soc.* **144**, 3517–3526 (2022).
11. S. S. Collins *et al.*, Plasmon energy transfer in hybrid nanoantennas. *ACS Nano* **15**, 9522–9530 (2021).
12. K. Wu, J. Chen, J. R. McBride, T. Lian, Efficient hot-electron transfer by a plasmon-induced interfacial charge-transfer transition. *Science* **349**, 632–635 (2015).
13. W. Yang, Y. Liu, D. A. Cullen, J. R. McBride, T. Lian, Harvesting sub-bandgap IR photons by photothermionic hot electron transfer in a plasmonic p-n junction. *Nano Lett.* **21**, 4036–4043 (2021).
14. A. Gellé *et al.*, Applications of plasmon-enhanced nanocatalysis to organic transformations. *Chem. Rev.* **120**, 986–1041 (2020).
15. E. L. Keller, R. R. Frontiera, Monitoring charge density delocalization upon plasmon excitation with ultrafast surface-enhanced Raman spectroscopy. *ACS Photon.* **4**, 1033–1039 (2017).
16. E. L. Keller, R. R. Frontiera, Ultrafast nanoscale raman thermometry proves heating is not a primary mechanism for plasmon-driven photocatalysis. *ACS Nano* **12**, 5848–5855 (2018).
17. N. C. Brandt, E. L. Keller, R. R. Frontiera, Ultrafast surface-enhanced Raman probing of the role of hot electrons in plasmon-driven chemistry. *J. Phys. Chem. Lett.* **7**, 3178–3185 (2016).
18. Z. Yu, R. R. Frontiera, Intermolecular forces dictate vibrational energy transfer in plasmonic-molecule systems. *ACS Nano* **16**, 847–854 (2022).
19. C. L. Warkentin, Z. Yu, A. Sarkar, R. R. Frontiera, Decoding chemical and physical processes driving plasmonic photocatalysis using surface-enhanced Raman spectroscopies. *Account. Chem. Res.* **54**, 2457–2466 (2021).
20. E. A. Sprague-Klein *et al.*, Photoinduced plasmon-driven chemistry in trans-1,2-Bis (4-pyridyl)ethylene gold nanosphere oligomers. *J. Am. Chem. Soc.* **140**, 10583–10592 (2018).
21. Y. Wu *et al.*, SERS study of the mechanism of plasmon-driven hot electron transfer between gold nanoparticles and PCBM. *J. Phys. Chem. C* **123**, 29908–29915 (2019).
22. Y. Qi *et al.*, Plasmon-driven chemistry in ferri-/ferrocyanide gold nanoparticle oligomers: A SERS study. *J. Am. Chem. Soc.* **142**, 13120–13129 (2020).
23. N. G. Greeneltch, M. G. Blaber, A. I. Henry, G. C. Schatz, R. P. Van Duyne, Immobilized nanorod assemblies: Fabrication and understanding of large area surface-enhanced Raman spectroscopy substrates. *Anal. Chem.* **85**, 2297–2303 (2013).
24. L. A. Dick, A. D. McFarland, C. L. Haynes, R. P. Van Duyne, Metal film over nanosphere (MFON) electrodes for surface-enhanced Raman spectroscopy (SERS): Improvements in surface nanostructure stability and suppression of irreversible loss. *J. Phys. Chem. B* **106**, 853–860 (2002).
25. S. S. Masango *et al.*, High-resolution distance dependence study of surface-enhanced raman scattering enabled by atomic layer deposition. *Nano Lett.* **16**, 4251–4259 (2016).
26. H. Feilchenfeld, G. Chumanov, T. M. Cotton, Photoreduction of methylviologen adsorbed on silver. *J. Phys. Chem.* **100**, 4937–4943 (1996).
27. S. H. Chen, X. M. Ren, SERS studies of methylviologen on silver sol and the effect of halide ions. *Spectrochim. Acta Part A: Mol. Spectrosc.* **51**, 717–725 (1995).
28. Q. Feng, W. Yue, T. M. Cotton, Surface-enhanced resonance Raman scattering from methylviologen at a silver electrode: Evidence for two distinct adsorption interactions. *J. Phys. Chem.* **94**, 2082–2091 (1990).
29. C. Fang, G. Wu, The relaxations of temporal bond polarizabilities of methylviologen adsorbed on the Ag electrode by 514.5 nm excitation: A Raman intensity study. *J. Raman Spectrosc.* **40**, 308–314 (2009).
30. A. J. Wilson, P. K. Jain, Light-induced voltages in catalysis by plasmonic nanostructures. *Acc. Chem. Res.* **53**, 1773–1781 (2020).
31. S. Zaleski *et al.*, Investigating nanoscale electrochemistry with surface- and tip-enhanced Raman spectroscopy. *Acc. Chem. Res.* **49**, 2023–2030 (2016).
32. L. Yu, A. Du, L. Yang, Y. Hu, W. Xie, Quantifying hot electron energy contributions in plasmonic photocatalysis using electrochemical surface-enhanced Raman spectroscopy. *J. Phys. Chem. Lett.* **13**, 5495–5500 (2022).
33. D. V. Chulhai, L. Jensen, Determining molecular orientation with surface-enhanced Raman scattering using inhomogenous electric fields. *J. Phys. Chem. C* **117**, 19622–19631 (2013).
34. A. di Matteo, Structural, electronic and magnetic properties of methylviologen in its reduced forms. *Chem. Phys. Lett.* **439**, 190–198 (2007).
35. S. Ghoshal, T. Lu, Q. Feng, T. M. Cotton, A normal coordinate analysis of the vibrational modes of the three redox forms of methylviologen: Comparison with experimental results. *Spectrochim. Acta Part A: Mol. Spectrosc.* **44**, 651–660 (1988).
36. Y. Fang, N. H. Seong, D. D. Dlott, Measurement of the distribution of site enhancements in surface-enhanced Raman scattering. *Science* **321**, 388–392 (2008).
37. A. J. Wilson, P. K. Jain, Structural dynamics of the oxygen-evolving complex of photosystem II in water-splitting action. *J. Am. Chem. Soc.* **140**, 5853–5859 (2018).
38. M. L. Brongersma, N. J. Halas, P. Nordlander, Plasmon-induced hot carrier science and technology. *Nat. Nanotechnol.* **10**, 25–34 (2015).

39. Y. Y. Cai *et al*., Anti-stokes emission from hot carriers in gold nanorods. *Nano Lett.* **19**, 1067–1073 (2019).
40. G. V. Hartland, Coherent excitation of vibrational modes in metallic nanoparticles. *Annu. Rev. Phys. Chem.* **57**, 403–430, PMID: 16599816 (2006).
41. S. L. Kleinman, R. R. Frontiera, A. I. Henry, J. A. Dieringer, R. P. V. Duyne, Creating, characterizing, and controlling chemistry with SERS hot spots. *Phys. Chem. Chem. Phys.* **15**, 21–36 (2013).
42. J. L. Brooks, D. V. Chulhai, Z. Yu, J. D. Goodpaster, R. R. Frontiera, Plasmon-driven C-N bond cleavage across a series of viologen derivatives. *J. Phys. Chem. C* **123**, 29306–29313 (2019).
43. J. J. Sun *et al*., Role of adsorption orientation in surface plasmon-driven coupling reactions studied by tip-enhanced Raman spectroscopy. *J. Phys. Chem. Lett.* **10**, 2306–2312 (2019).
44. R. W. Schoenlein, W. Z. Lin, J. G. Fujimoto, G. L. Eesley, Femtosecond studies of nonequilibrium electronic processes in metals. *Phys. Rev. Lett.* **58**, 1680–1683 (1987).
45. A. Turchanin *et al*., Molecular mechanisms of electron-induced cross-linking in aromatic SAMs. *Langmuir* **25**, 7342–7352 (2009).
46. D. S. Wastl, A. J. Weymouth, F. J. Giessibl, Optimizing atomic resolution of force microscopy in ambient conditions. *Phys. Rev. B - Condens. Matter Mater. Phys.* **87**, 245415 (2013).
47. J. L. Brooks, R. R. Frontiera, Competition between reaction and degradation pathways in plasmon-driven photochemistry. *J. Phys. Chem. C* **120**, 20869–20876 (2016).
48. H. Shiraishi, G. V. Buxton, N. D. Wood, Temperature dependence of the absorption spectrum of the methyl viologen cation radical and use of methyl viologen as a scavenger for estimating yields of the primary radicals in the radiolysis of high-temperature water. *Int. J. Radiat. Appl. Inst. Part C. Radiat. Phys. Chem.* **33**, 519–522 (1989).
49. R. R. Frontiera, A. I. Henry, N. L. Gruenke, R. P. V. Duyne, Surface-enhanced femtosecond stimulated Raman spectroscopy. *J. Phys. Chem. Lett.* **2**, 1199–1203 (2011).
50. E. Contreras *et al*., Plasmon-assisted ammonia electrosynthesis. *J. Am. Chem. Soc.* **144**, 10743–10751 (2022).
51. H. Reddy *et al*., Determining plasmonic hot-carrier energy distributions via single-molecule transport measurements. *Science* **369**, 423–426 (2020).
52. D. M. Collard, M. A. Fox, Use of electroactive thiols to study the formation and exchange of alkanethiol monolayers on gold. *Langmuir* **7**, 1192–1197 (1991).
53. Y. Xue, X. Li, H. Li, W. Zhang, Quantifying thiol-gold interactions towards the efficient strength control. *Nat. Commun.* **5**, 4348 (2014).
54. H. Häkkinen, The gold-sulfur interface at the nanoscale. *Nat. Chem.* **4**, 443–455 (2012).
55. D. Mollenhauer, N. Gaston, E. Voloshina, B. Paulus, Interaction of pyridine derivatives with a gold (111) surface as a model for adsorption to large nanoparticles. *J. Phys. Chem. C* **117**, 4470–4479 (2013).
56. L. Stolberg, S. Morin, J. Lipkowski, D. E. Irish, Adsorption of pyridine at the Au(111)-solution interface. *J. Electr. Chem.* **307**, 241–262 (1991).
57. A. Bilić, J. R. Reimers, N. S. Hush, Adsorption of pyridine on the gold(111) surface: Implications for "alligator clips" for molecular wires. *J. Phys. Chem. B* **106**, 6740–6747 (2002).
58. J. M. Beebe, V. B. Engelkes, L. L. Miller, C. D. Frisbie, Contact resistance in metal-molecule-metal junctions based on aliphatic SAMs: Effects of surface linker and metal work function. *J. Am. Chem. Soc.* **124**, 11268–11269 (2002).
59. O. T. Hofmann *et al*., Orientation-dependent work-function modification using substituted pyrene-based acceptors. *J. Phys. Chem. C* **121**, 24657–24668 (2017).
60. C. L. Warkentin, R. R. Frontiera, Quantifying the ultrafast and steady-state molecular reduction potential of a plasmonic photocatalyst – data and analysis files, collected in 2022. Data Repository for U of M. https://hdl.handle.net/11299/255747. Deposited 3 August 2023.